Journal of Visual Communication and Image Representation **11**, 196–208 (2000)
doi:10.1006/jvci.1999.0445, available online at http://www.idealibrary.com on IDEAL®

Applications of Locally Orderless Images

Bram van Ginneken and Bart M. ter Haar Romeny[1]

Image Sciences Institute, Utrecht University, The Netherlands
E-mail: bram@isi.uu.nl, bart@isi.uu.nl

Received September 21, 1999; revised November 14, 1999

In a recent work, J. J. Koenderink and A. J. Van Doorn considered a family of three intertwined scale-spaces coined the locally orderless image (LOI) (1999, *J. Comput. Vision*, **31** (2/3), 159–168). The LOI represents the image, observed at inner scale σ, as a local histogram with bin-width β, at each location, with a Gaussian-shape region of interest of extent α. LOIs form a natural and elegant extension of scale-space theory, show causal consistency, and enable the smooth transition between pixels, histograms, and isophotes. The aim of this work is to demonstrate the wide applicability and versatility of LOIs. We present applications for a range of image processing tasks, including new nonlinear diffusion schemes, adaptive histogram equalization and variations, several methods for noise and scratch removal, texture rendering, classification, and segmentation.

Key Words: scale-space; local histograms.

1. INTRODUCTION

Histograms are ubiquitous in image processing. They embody the notion that for many tasks the intensity distribution within a region of interest contains the required information, with the spatial order of the pixels being immaterial. One can argue that even at a single location (which is a physical impossibility since any measurement is of nonzero scale) the intensity has an uncertainty and should therefore be described by a probability distribution: physical plausibility requires nonzero imprecision. This led Griffin [9] to propose a *scale-imprecision space* with spatial scale parameter σ and an intensity, or tonal scale β, which can be identified as the familiar *bin-width* of histograms.

Koenderink and Van Doorn [15] extended this concept to *locally orderless images* (LOIs), an image representation with three scale parameters in which there is no local but only a global topology defined. LOIs are *local histograms*, constructed according to scale-space principles, viz. without violating the causality principle. As such, one can apply to LOIs the whole machinery of techniques that has been developed in the context of scale-space research, such as the N-jet for local image structure description, the construction of invariants and (oriented) filter families, nonlinear diffusion schemes, and scale selection methods.

[1] URL: http://www.isi.uu.nl/.

1047-3203/00 $35.00

In this paper, we aim to demonstrate that LOIs are a versatile and flexible framework for image processing applications. The reader may conceive this article as a broad feasibility study. Due to space limitations, we cannot give thorough evaluations for each of the applications presented. Obviously, local histograms are in common use in many areas, and the notion of considering histograms at different scales (soft binning) is not new either. Yet we believe that the use of a consistent mathematical framework in which all scale parameters are made explicit can aid in the design of effective algorithms by reusing existing scale-space concepts. Additional insight may be gained by taking into account the behavior of LOIs over scale.

2. LOCALLY ORDERLESS IMAGES

We first briefly review locally orderless images [15] and comment on some interesting attributes. A convenient introduction is to consider the scale parameters involved in the calculation of a histogram:

- the inner scale σ with which the image is observed;
- the outer scale, or extent, or scope α that parameterizes the size of the field of view over which the histogram is calculated;
- the scale at which the histogram is observed, tonal scale, or bin-width β.

The locally orderless images $H(\mathbf{x_0}, i; \sigma, \alpha, \beta)$ are defined as the family of histograms, i.e., a function of the intensity i, with bin-width β of the image observed at scale σ calculated over a field of view centered around $\mathbf{x_0}$ with an extent α. The unique way to decrease resolution without creating spurious resolution is by convolution with Gaussian kernels [14, 24]. Therefore Gaussian kernels are used for σ, α, and β.

We summarize this with a recipe for calculating LOIs:

1. Choose an inner scale σ and blur the image $L(x; \sigma)$ using the diffusion

$$\Delta_{(\mathbf{x})} L(\mathbf{x}; \sigma) = \frac{\partial L(\mathbf{x}; \sigma)}{\partial \frac{\sigma^2}{2}}. \tag{1}$$

2. Choose a number of (equally spaced) bins of intensity levels i and calculate the soft isophote images, representing the stuff in each bin through the Gaussian gray-scale transformation

$$R(\mathbf{x}, i; \sigma, \beta) = \exp\left(-\frac{(L(\mathbf{x}; \sigma) - i)^2}{2\beta^2}\right). \tag{2}$$

3. Choose a scope α for a Gaussian aperture, normalized to unit amplitude

$$A(\mathbf{x}; \mathbf{x_0}, \alpha) = \exp \frac{-(\mathbf{x} - \mathbf{x_0})(\mathbf{x} - \mathbf{x_0})}{2\alpha^2} \tag{3}$$

and compute the locally orderless image through convolution

$$H(\mathbf{x_0}, i; \sigma, \alpha, \beta) = \frac{A(\mathbf{x}; \mathbf{x_0}, \alpha)}{2\pi\alpha^2} * R(\mathbf{x}, i; \sigma, \beta). \tag{4}$$

Note that $H(\mathbf{x_0}, i; \sigma, \beta, \alpha)$ is a stack of isophote images and therefore has a dimensionality 1 higher than that of the input image.

4. The bin-width β can be increased by keeping $\mathbf{x_0}$, σ, and α fixed and blurring along the intensity direction:

$$\frac{\partial^2 H(\mathbf{x_0}, i; \sigma, \alpha, \beta)}{\partial i^2} = \frac{\partial H(\mathbf{x_0}, i; \sigma, \alpha, \beta)}{\partial \frac{\beta^2}{2}}. \tag{5}$$

5. The extent α can be increased by keeping i, σ, and β fixed and blurring each intensity slice:

$$\Delta_{(\mathbf{x_0})} H(\mathbf{x_0}, i; \sigma, \alpha, \beta) = \frac{\partial H(\mathbf{x_0}, i; \sigma, \alpha, \beta)}{\partial \frac{\alpha^2}{2}}, \tag{6}$$

The term locally orderless image refers to the fact that we have at our disposal at each location the probability distribution, which is a mere orderless set; the spatial structure within the field of view α centered at $\mathbf{x}$ has been completely disregarded. This is the key point: with each spatial location we no longer associate a (scalar) intensity, but rather a probability distribution, parameterized by σ, α, β. Since a distribution contains more information than the intensity sec, we may expect to be able to use this information in various image processing tasks.

The LOI contains several conventional concepts, such as the original image and its scale-space $L(\mathbf{x}; \sigma)$ that can be recovered from the LOI by integrating $i\,H(\mathbf{x_0}, i; \sigma, \alpha, \beta)$ over i. The image histogram in the conventional sense is obtained by letting $\alpha \to \infty$. The construction also includes families of isophote images, which for $\beta > 0$ are named *soft isophote images* by Koenderink. And maybe even more important, by tuning the scale parameters the LOI can fill intermediate stages between the image, its histogram, and its isophotes. This can be useful in practice. Finally, we note that the framework generalizes trivially to nD images or color images, if a color metric is selected.

3. MEDIAN AND MAXIMUM MODE EVOLUTION

If we replace the histogram at each location with its mean, we obtain the input image $L(\mathbf{x}; \sigma)$ blurred with a kernel with width α. This holds independent of β, since blurring a histogram does not alter its mean. If, however, we replace the histogram with its median or its maximum mode (the intensity with the highest probability), we obtain a diffusion with scale parameter α that is reminiscent of some nonlinear diffusion schemes (see Fig. 1). In fact it has been shown by Guichard and Morel [10] that mean curvature flow corresponds to iterated median filtering, but the relation between other histogram operations and nonlinear diffusion schemes is less clear. The tonal scale β works as a tuning parameter that determines the amount of nonlinearity. Griffin [9] proved that for infinite imprecision ($\beta \to \infty$) median filtering corresponds to linear filtering. With only a few soft isophote level images in the LOI, maximum mode diffusion also performs some sort of quantizing, and one obtains piecewise homogeneous patches with user-selectable values. This can be useful, e.g., in coding for data compression and knowledge driven enhancements.

4. SWITCHING MODES IN BIMODAL HISTOGRAMS

Instead of replacing each pixel with a feature of its local histogram, such as the median or the maximum mode, we can perform more sophisticated processing if we take the structure of the local histograms into account. If this histogram is bimodal, this indicates the presence

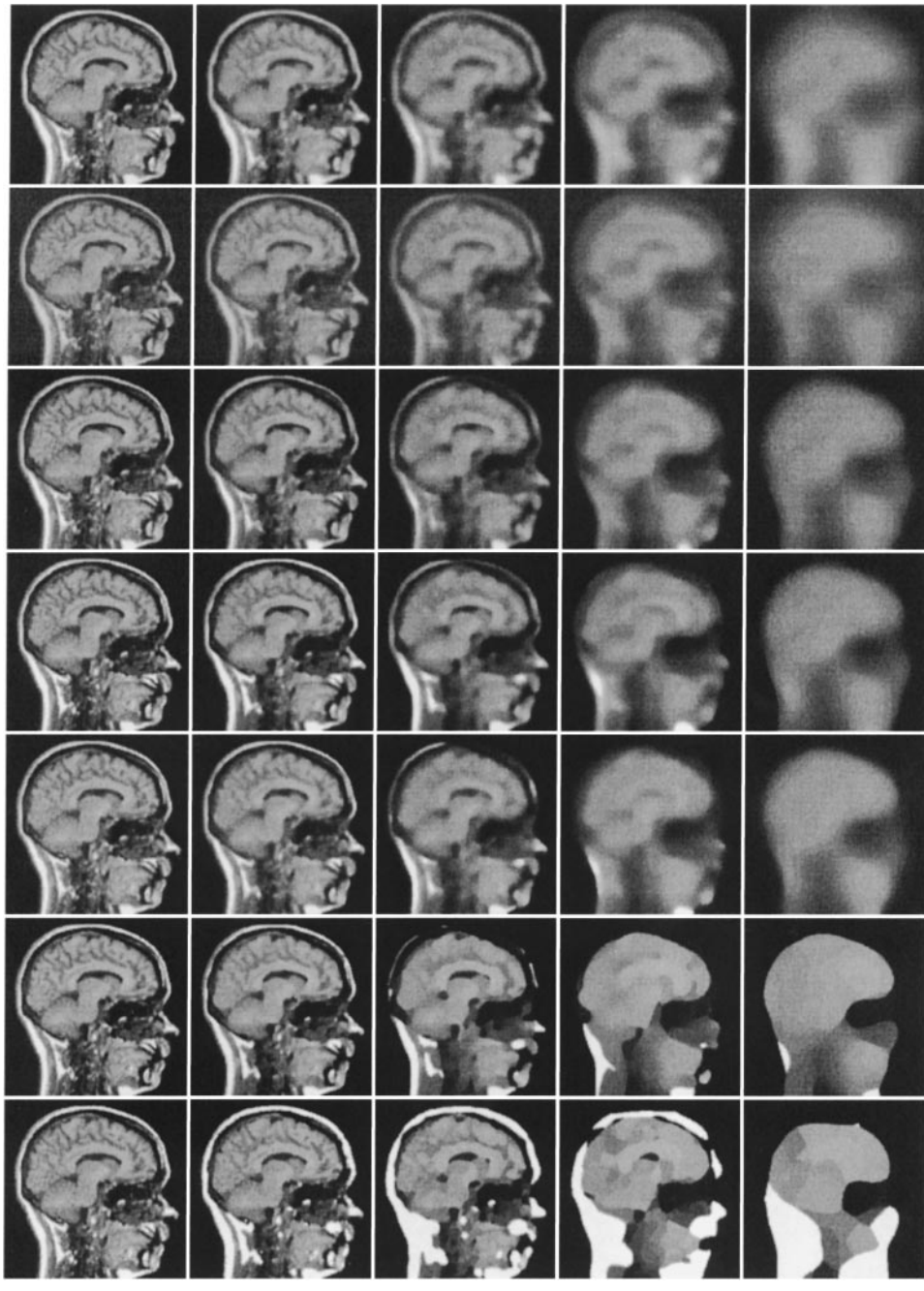

FIG. 1. Input image is a sagittal 256×256 MR brain image with intensities in the range [0, 255]. Each row shows a diffusion of the LOI with $\sigma = 0$ for $\alpha = 1, 2, 4, 8, 16$. Top row: mean diffusion, equivalent to linear scale space. Rows 2 to 4: median diffusion for $\beta = 64, 16, 1$. Rows 5 to 7: global mode diffusion for $\beta = 64, 16, 1$.

of multiple objects in the neighborhood of that location. Noest and Koenderink [18] have suggested dealing with partial occlusion in this way.

Consider locations with bimodal histograms (histograms with two maxima, with a single minimum in between). We let pixels at such locations switch to a desired mode. That is, if

FIG. 2. Left: Text hidden in a sinusoidal background, dimensions 230×111, intensities in the range [0, 1]. Middle: bimodal locations in an LOI of $\sigma = 0$, $\beta = 0.15$, and $\alpha = 1.5$. Right: bimodal locations have been replaced with the high mode. Text is removed and the background restored.

they are in the high mode (their value is higher than that of the minimum in between the two modes), we replace their value with the low mode (or vice versa, depending on the desired effect). The idea behind this is that a bright (dark) object is replaced with the most likely value that the darker (brighter) object that surrounds it has, namely the low (high) maximum mode. Note that this a two-step process: the detection of bimodal locations is a segmentation step, and replacing pixels fills in a value from its surroundings, thus using statistical information and taking into account only those pixels that belong to the object to be filled in.

This scheme allows for a scale-selection procedure in the following way. For fixed σ, β, α, there may be locations with more than two modes in their local distribution. This indicates that it is worthwhile to decrease α, focusing on a smaller neighborhood, until just two modes remain. Thus we use a locally adaptive α, ensuring that the replaced pixel value comes from information from locations as close as possible to the pixel to be replaced.

We have applied this scheme successfully for the removal of text on a complicated background (Fig. 2), the detection of dense objects in chest radiographs, and noise removal. Figure 3 shows how shot noise can be detected and replaced with a probable value, obtained

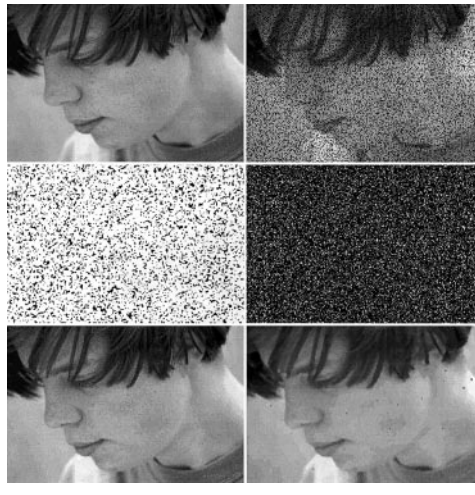

FIG. 3. (Top-left) Original image, 400×267 pixels, intensities scaled to [0, 1]; (top-right) Original image with 20% shot noise. This is the input image for the restoration procedure. A LOI with $\sigma = 0$, $\beta = 0.04$, $\alpha = 0.4$ was computed. (Middle-left) Binary image with locations in top-right image with bimodal histograms shown in white. (Middle-right) Binary image with locations in top-right image with bimodal histograms and pixels in the low mode shown in white. These locations are replaced. (Bottom-left) Restoration using mode-switching for bimodal locations gives excellent results; (bottom-right) Restoration using a 5×5 median filter removes most, but not all shot noise, and blurs the image.

from the local histogram. The restoration is near perfect. We also applied the mode switching technique on old movie sequences with severe deteriorations and could automatically remove most artifacts. In order to avoid finding local bimodal locations due to movement between the image frames, we considered for this case two LOIs, one in which the frame to be restored was the first and one in which it was the last image. Only those locations that were bimodal in both cases were taken in consideration.

5. HISTOGRAM TRANSFORMATIONS

Any generic histogram can be transformed into any other histogram by a nonlinear, monotonic gray-level transformation. To see this, consider an input histogram $h_1(i)$ and its cumulative histogram $\int_{-\infty}^{i} h_1(i')\,di' = H_1(i)$ and the desired output histogram $h_2(i)$ and $H_2(i)$. If we replace every i with the i' for which $H_1(i) = H_2(i')$ we have transformed the cumulative histogram H_1 into H_2 and thus also h_1 into h_2. Since cumulative histograms are monotonically increasing, the mapping is monotonically increasing as well.

Although in practice this can only be achieved to limited accuracy due to discretization of the intensity domain, histogram manipulation is a very useful technique if one has an idea of what the output histogram as a function of the input histogram should be.

Histogram equalization is an example. The idea is that when displaying an image with a uniform histogram (within a certain range), all available gray levels or colors will be used in equal amounts and thus perceptual contrast is maximal. The idea to use local histograms (that is, selecting a proper α for the LOI) for equalization, to obtain optimal contrast over each region in the image stems from the 1970s [13] and is called *adaptive histogram equalization* (AHE). However, it was noted that these operations blow up noise in homogeneous regions. Pizer *et al.* [20] proposed to *clip* histograms, viz. for each bin with more pixels than a certain threshold, truncate the number of pixels and redistribute these uniformly over all other bins. It can be seen that this ad hoc technique amounts to the same effect as increasing β in the LOI; notably, for $\beta \to \infty$, AHE has no effect. Thus we see that the two scale parameters α and β determine the size of structures that are enhanced and the amount of enhancement, respectively. Figure 4 shows a practical example of such a continuously tuned AHE for a medical modality (thorax X-ray) with a wide latitude of intensities.

An alternative to histogram equalization is to increase the standard deviation of the histogram by a constant factor, which can be done by a linear gray-level transformation or variations on such schemes [4]. Again, the LOI provides us with an elegant framework in which the scale parameters that determine the results of such operations are made explicit.

Another application of histogram transformation is to approximate changes in texture due to different viewing and illumination directions [8]. In general, the textural appearance of many common real-world materials is a complex function of the light field and viewing position. In computer graphics it is common practice, however, to simply apply a projective transformation to a texture patch in order to account for a change in viewing direction and to adjust the mean brightness using a bidirectional reflection distribution function (BRDF), often assumed to be simply Lambertian. In [8] it is shown that this gives poor results for many materials and that histogram transformations often produce far more realistic results. A logical next step is to consider local histogram transformations. An example is shown in Fig. 5, using a texture of rough concrete taken from the CURET database [5]. Instead of using one mapping function for all pixel intensities, the mapping is now based on the pixel

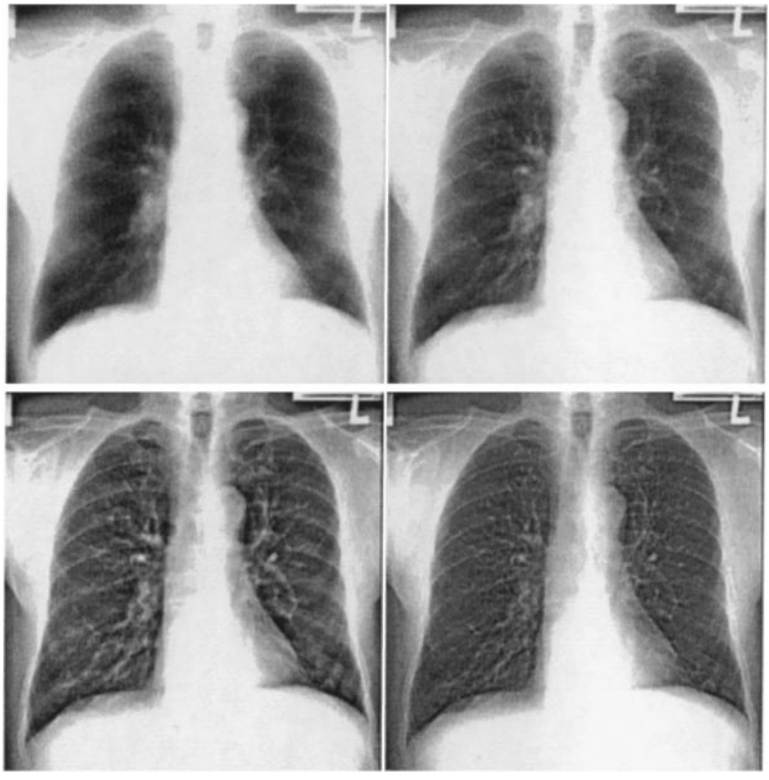

FIG. 4. A normal PA chest radiograph of 512×512 pixels with intensities in the range [0, 1]. (Top-left) Original image, in which details in lung regions and mediastinum are not well visible due to the large dynamic range of gray levels. (Top-right) AHE based on the LOI with $\sigma = 0$, $\alpha = 8$; $\beta = 0.4$. (Bottom-left) AHE with $\sigma = 0$, $\alpha = 8$; $\beta = 0.2$. (Bottom-right) AHE with $\sigma = 0$, $\alpha = 4$; $\beta = 0.2$.

intensity and the intensities in its surroundings. Simple physical considerations make clear that this approach does make sense: bright pixels which have dark pixels due to shadowing in their neighborhood are more likely to become shadowed for more oblique illumination than those that are in the center of a bright region.

Finally, histogram transformations can be applied to restore images that have been corrupted by some noise process, but for which the local histogram properties are known or can be estimated from the corrupted image. Although this may sound contrived, we believe such cases are encountered frequently in practice. Many image acquisition systems contain artifacts that are hard to correct with calibration schemes. One example in medical image processing is the inhomogeneity of the magnetic field of an MR scanner or of the sensitivity of MR surface coils, leading to low frequency gradients over the image. A generated example is shown in Fig. 6 where we multiplied a texture image with Gaussian noise. We make two assumptions: (1) the noise does not contain high frequency components and thus the structure of the local histogram will not be affected for a small scope α; (2) the original texture image has small textons, so that over a small scope, the histograms are equal everywhere. By randomly choosing a point in the corrupted image and computing the mapping that transforms each local histogram to the local histogram at that particular location we obtain the restored image in Fig. 6d. The texture of the restored image is more uniform than in the original, indicating that assumption (2) is not completely valid. Furthermore, in areas

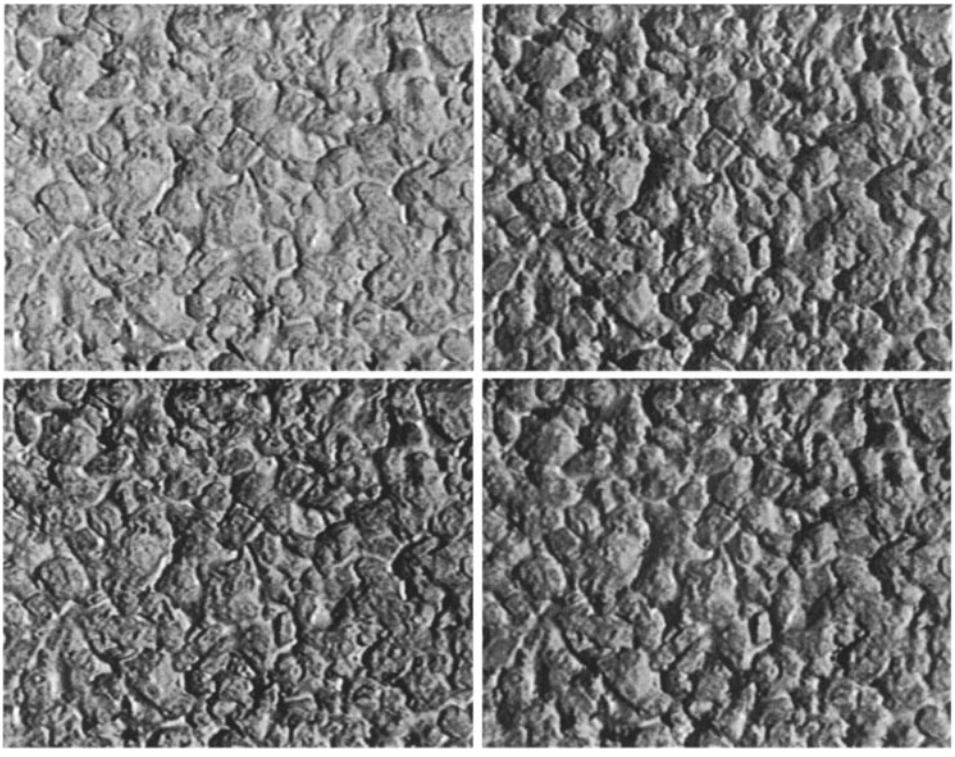

FIG. 5. (Top-left) Image (332×259 pixels) of rough concrete viewed frontally, illuminated from 22°. (Top-right) The same material illuminated from 45°. (Bottom-left) Top-left image with its histogram mapped to the top-right image to approximate the change in texture. (Bottom-right) Result of local histogram transformation, with $\alpha = 2$. The approximation is especially improved in areas that show up white in the images on the left. These areas are often partly shadowed with illumination from 45°, and using a local histogram may correctly predict such transitions.

where the noise factor with which the texture was multiplied was close to 0, all information is destroyed and restoration fails. Note that we did not make any assumption about the noise process. In this particular case, dividing Fig. 6 with a median filtered version of it would give good restoration as well, but this assumes corruption by multiplicative noise. The LOI method works for additive noise or other kinds of noise as well.

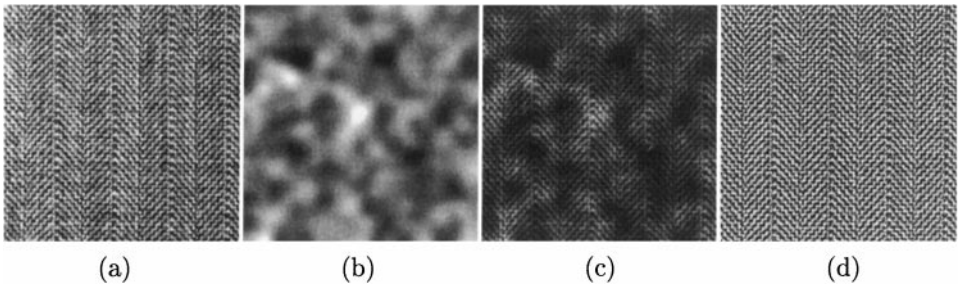

FIG. 6. (a) A texture from the Brodatz set [3], resolution 256^2, intensities in the range [0, 1]. (b) Blurred Gaussian noise, scaled to range from [0, 1]. (c) Multiplication of (a) and (b). (d) Reconstruction of (a) from (c) from the LOI with $\sigma = 0$, $\beta = 0.1$, $\alpha = 2$ and computing for each point a mapping to the local histogram at the randomly chosen location (80, 80).

6. TEXTURE CLASSIFICATION AND DISCRIMINATION

LOIs can be used to set up a framework for classification or discrimination of textures. The histogram is one of the simplest texture descriptions; the spatial structure has been completely disregarded and only the probability distribution remains. This implies that any feature derived from LOIs is rotationally invariant and thus unable to discriminate between patches of, let us say, horizontal and vertical stripes. There are several ways possible to extend LOIs:

- *Locally orderless derivatives:* Instead of using $L(\mathbf{x};\sigma)$ as input for the calculation of LOIs, we can use $L_n^{\theta}(\mathbf{x};\sigma)$, which denotes the nth order spatial derivative of the image at scale σ in the direction θ. These images can be calculated for any θ from a fixed set of basis filters in several ways; for a discussion see [6, 19]. For $n=0$, these locally orderless derivatives (LODs) reduce to the LOIs. Alternatively, one could choose another family of filters instead of directional derivatives of Gaussians, such as differences of offset Gaussians [17, 21] or Gabor filters [2].
- *Directional locally orderless images:* Another way to introduce orientation sensitivity in LOIs is to use anisotropic Gaussians as local regions of interest. This would extend the construction with an orientation $0<\theta<\pi$ and an anisotropy factor.
- *Cooccurrence matrices:* Haralick [11, 12] introduced cooccurrence matrices, which are joint probability densities for locations at a prescribed distance and orientation. Texture features can be computed from these matrices. It is straightforward to modify the LOIs into a construction equivalent to cooccurrence matrices. It leads to joint probability functions as a function of location. For $\alpha=0$, each joint probability function is a two-dimensional Gaussian with width β.

Results from psychophysics suggest that if two textures T_1 and T_2 are to be preattentively discriminable by human observers, they must have different spatial average $\int_{T_1} R(x,y)$ and $\int_{T_2} R(x,y)$ of some locally computed neural response R [17]. We use this as a starting point and we will compute features derived from LODs and average these over texture patches. Averaging will give identical results for any α if we use linear operations on LODs to compute local features. Thus we include nonlinear operations on the local histograms as well. An obvious choice is to use higher order moments. The strategy to derive features from the histograms of filtered versions of textures is common in texture analysis [16, 22], but the effectiveness of a scheme that generates features by systematically varying σ, α, β has not been researched before.

Which combinations of scales are interesting to select? First of all, we should have $\sigma<\alpha$; otherwise local histograms are peaked distributions and higher order moments of these distributions are fully predictable. Furthermore, in practice σ and β will often be mutually exclusive. Haralick [12] defined texture as a collection of (several distinguishable) typical elements, called tonal primitives or textons, put together according to certain placement rules. If we follow this definition, we can make some educated guesses as to which scales are interesting to consider. First, as the scope α is much larger than the spatial size of the textons, the local histograms will not change much anymore. Therefore it does not make sense to consider more than one LOI with α much larger than the texton size. Using $\alpha=\infty$ is the obvious choice for this large scope histogram. Second, if we vary σ at values below the texton size, we study the spatial structure of the textons. For σ much larger than the texton size, we are investigating the characteristics of the placement rules.

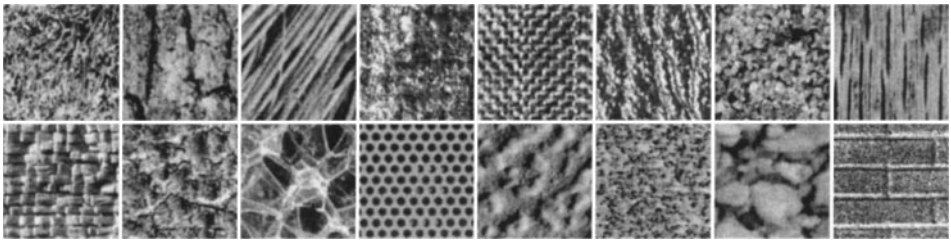

FIG. 7. The 16 different textures used in a texture classification experiment.

We performed an experiment using texture patches from 16 large texture images from the USC-SIPI database [23], 11 of which originated from the Brodatz collection [3]. From each texture, 16 nonoverlapping regions were cropped and subsampled to a resolution of 128×128. Criteria for the size of the cropped regions were that several textons should be visible in the texture patch. Intensity values of each patch were normalized to zero mean and unit variance. Figure 7 shows one patch for each texture class.

We classified with the nearest-neigbor rule and the leave-one-out method (see, e.g., [7]). A small set of nine features was already able to classify 255 out of 256 textures correctly. This set consisted of three input images, $L_0(\mathbf{x}; \sigma = 0)$ (used in features 1–3), $L_1^{0^\circ}(\mathbf{x}; \sigma = 1)$ (used in features 4–6), and $L_0^{90^\circ}(\mathbf{x}; \sigma = 1)$ (used in features 7–9) for which we calculated the averaged second moment (viz. the local standard deviation) for $\beta = 0.1$ and $\alpha = 1, 2, \infty$.

To gain more insight into the discriminative power of each of the calculated features separately, we performed the classification for any possible combination of one, two, or three out of the nine features. The best and worst results are given in Table I. It is interesting to see that there is no common feature in the best single set, the best two features, and the three best ones, which indicates that all features contain discriminant power, except maybe for feature 3. Note that since we use only second order moments, features are invariant to gray-level inversion. This can be solved by adding third and higher order moments to the feature set, which was apparently unnecessary for the test set considered.

7. TEXTURE SEGMENTATION BASED ON LOCAL HISTOGRAMS

Many general (semi-)automatic segmentation schemes are based on the notion that points in spatial proximity with similar intensity values are likely to belong to the same object. Such methods have problems with textured areas, because the intensity values may show wild local variations. A solution is to locally compute texture features and replace pixel

TABLE I
Classification Results for Various Combinations of Features

	Features used	Result
Best single feature	7	47.6%
Worst single feature	3	12.9%
Best two features	4, 9	91.4%
Worst two features	2, 3	41.0%
Best three features	1, 5, 8	99.2%
Worst three features	3, 8, 9	71.5%
Nine features	All	99.6%

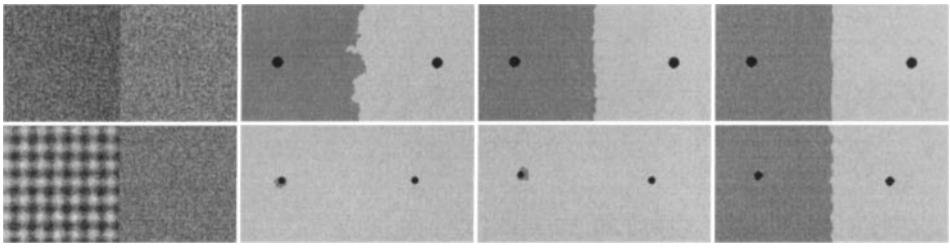

FIG. 8. (Top row, from left to right) A 256×128 test image composed of two homogenous regions with intensity 0 and 1 and Gaussian noise with zero mean and unit variance. An LOI with $\sigma = 0$ and $\beta = 0.2$ and $\alpha = 0$, 1, 4, respectively, is used for seeded region growing from the two seeds shown in white. Since the mean of the two regions is different, regular seeded region growing ($\alpha = 0$) works well. (Bottom row) Same procedure for a partly textured image; the left half was filled with $\sin(x/3) + \sin(y/3)$, the right half was set to zero, and Gaussian noise with zero mean and $\sigma = 0.5$ was added. Regular seeded region growing now fails, but if α is large enough, the segmentation is correct.

values with these features, assuming that pixels that belong to the same texture region will now have a similar value. The framework of LOIs is ideally suited to be used for the computation of such local features. One could use LODs or another extension of LOIs put forward in the previous section. Shi and Malik [21] have applied their normalized cut segmentation scheme to texture segmentation in this way, using local histograms and the correlation between them as a metric.

Here we present an adapted version of a semi-automatic segmentation technique called seeded region growing (SRG), developed by Adams and Bischof [1], that is popular in medical image processing. An attractive property of our adaptation of this scheme is that it reduces to a scheme very similar to the original SRG scheme for $\alpha \to 0$. This is directly due to the fact that LOIs contain the original image.

SRG segments an image starting from (user-selected or in some way automatically determined) seeds. The algorithm maintains a list of all pixels that are connected to one of the seeds, sorted according to the distance of the pixel to the seed. This metric is originally defined as the intensity of the pixel minus the mean intensity of the seed region squared. The pixel at the top of the list is added to the seed-region it is connected to, the mean intensity of this region is updated, and the neighbors of the added pixel are added to the list. This procedure is repeated, usually until all pixels are assigned to a region.

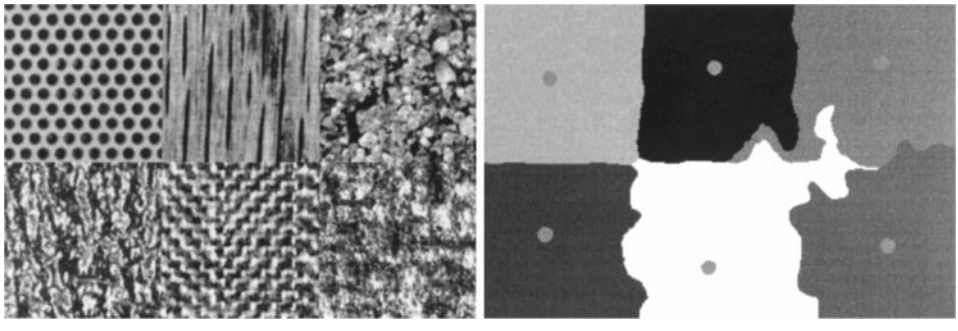

FIG. 9. (Left) A test image composed of six texture patches of pixel size 128×128 each. Intensity values in each patch are normalized to zero mean and unit variance. (Right) The result of segmentation with seeded region growing based on a LOI with $\sigma = 0$, $\beta = 0.2$, and $\alpha = 8$. The circles are the seeds.

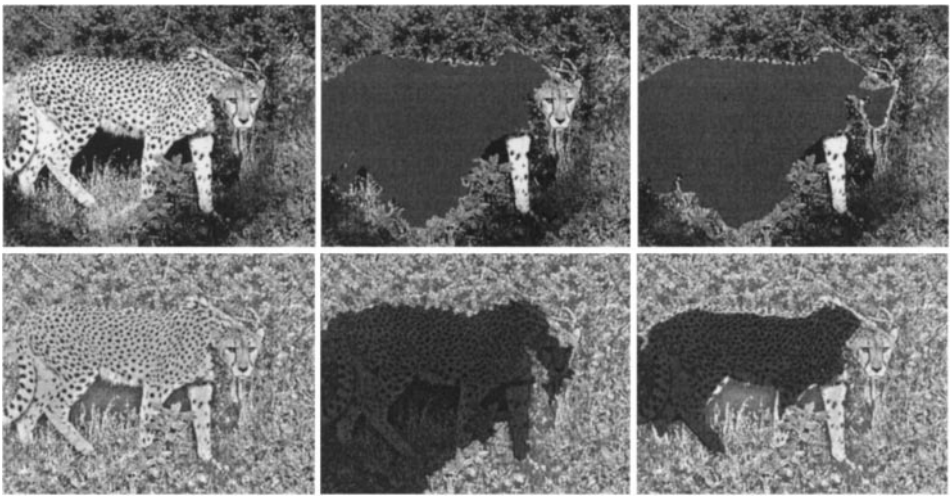

FIG. 10. (Top row, left) Wildlife scene with leopard, size 329×253 pixels, intensities scaled between [0, 1]; (Bottom row, left) A locally ($\sigma = 8$) normalized version of the input image. (Middle and right) Segmentation by SRG based upon LOI with $\sigma = 0$, $\beta = 0.05$, and $\alpha = 0, 4$, respectively. Note how well the textured area is segmented in the lower right image.

Instead of comparing pixel intensities values with the mean intensity of a region, we compare the local histograms of a pixel and a region. There are several ways in which one can implement the notion of a distance between two distributions. We choose to subtract the histograms and take the sum of the absolute values of what is left in the bins. For $\alpha \to 0$ this reduces to a scheme similar to the original scheme, except that one considers for the region the global mode instead of the mean of the histogram (most likely pixel value instead of the mean pixel value). Figures 8 to 10 illustrate the use of seeded region growing based on local histograms.

8. CONCLUDING REMARKS

In the applications presented, we have used many aspects of LOIs. In some cases, they are a natural extension ($\alpha > 0$) of techniques that usually use pixels ($\alpha = 0$), e.g., seeded region growing. In other cases, they extend techniques that use conventional histograms ($\alpha \to \infty$) with an extra parameter, e.g., histogram transformation techniques. Other applications exploit the behavior of LOIs over scale to obtain nonlinear diffusions, to do automatic scale selection in noise removal, and to derive texture features for classification. We conclude that LOIs are image representations of great practical value.

ACKNOWLEDGMENTS

This work is supported by the IOP Image Processing funded by the Dutch Ministry of Economic Affairs.

REFERENCES

1. R. Adams and L. Bischof, Seeded region growing, *IEEE Trans. Pattern Anal. Mach. Intell.* **16**, 1994, 641–647.
2. A. C. Bovik, M. Clark, and W. S. Geisler, Multichannel texture analysis using localized spatial filters, *IEEE Trans. Pattern Anal. Mach. Intell.* **12**, 1990, 55–73.

3. P. Brodatz, *Textures*, Dover, New York, 1966.
4. D. C. Chan and W. R. Wu, Image contrast enhancement based on a histogram transformation of local standard deviation, *IEEE Trans. Med. Imaging* **17**, 1998, 518–531.
5. K. J. Dana, B. van Ginneken, S. K. Nayar, and J. J. Koenderink, Reflectance and texture of real-world surfaces, *ACM Trans. Graphics* **18**, 1999, 1–34.
6. W. T. Freeman and E. H. Adelson, The design and use of steerable filters, *IEEE Trans. Pattern Anal. Mach. Intell.* **13**, 1991, 891–906.
7. K. Fukunaga, *Introduction to Statistical Pattern Recognition*, 2nd edition, Academic Press, San Diego, 1990.
8. B. van Ginneken, J. J. Koenderink, and K. J. Dana, Texture histograms as a function of illumination and viewing direction, *Internat. J. Comput. Vision* **31**(2/3), 1999, 169–184.
9. L. D. Griffin, Scale-imprecision space, *Image Vision Comput.* **15**, 1997, 369–398.
10. F. Guichard and J. M. Morel, Partial differential equations and image iterative filtering, in *State of the Art in Numerical Analysis*, Oxford University Press, Oxford, 1997.
11. R. M. Haralick, K. Shanmugam, and I. Dinstein, Textural features for image classification, *IEEE Trans. Systems, Man Cybernet.* **3**, 1973, 610–621.
12. R. M. Haralick, Statistical and structural approaches to texture, *Proc. IEEE* **67**, 1979, 786–804.
13. R. A. Hummel, Image enhancement by histogram transformation, *Comput. Graphics Image Process.* **6**, 1977, 184–195.
14. J. J. Koenderink, The structure of images, *Biol. Cybernet.* **50**, 1984, 363–370.
15. J. J. Koenderink and A. J. van Doorn, The structure of locally orderless images, *Internat. J. Comput. Vision* **31**(2/3); 1999, 159–168.
16. K. D. Laws, *Textures Image Segmentation*, Ph.D. thesis, University of Southern California, 1980. Report 940.
17. J. Malik and P. Perona, Preattentive texture discrimination with early vision mechanisms, *J. Opt. Soc. Amer. A* **7**, 1990, 923–932.
18. A. J. Noest and J. J. Koenderink, Visual coherence despite transparency or partial occlusion, *Perception* **19**, 1990, 384.
19. P. Perona, Deformable kernels for early vision, *IEEE Trans. Pattern Anal. Mach. Intell.* **17**, 1995, 488–499.
20. S. M. Pizer, E. P. Amburn, J. D. Austin, R. Cromartie, A. Geselowitz, T. Greer, B. M. Ter Haar Romeny, J. Zimmerman, and K. Zuiderveld, Adaptive histogram equalization and its variations, *Comput. Vision Graphics Image Process.* **39**, 1987, 355–368.
21. J. Shi and J. Malik, Self inducing relational distance and its application to image segmentation, in *ECCV, 1998*.
22. M. Unser, Local linear transforms for texture measurements, *Signal Process.* **11**, 1986, 61–79.
23. A. G. Weber, *The Isc-Sipi Image Database*, Technical report, University of Southern California, 1997. [http://sipi.usc.edu]
24. J. Weickert, S. Ishikawa, and A. Imiya, On the history of Gaussian scale-space axiomatics, in *Gaussian Scale-Space Theory* (J. Sporring, M. Nielsen, L. Florack, and P. Johansen, Eds.), pp. 45–59, Kluwer, Dordrecht, 1997.